

## Growth, Vibrational and Thermal Studies on Melaminium Phthalate Single Crystals

Sangeetha Viswanathan,<sup>1</sup> Kanagathara Narayanan,<sup>2</sup> Mariusz K. Marchewka,<sup>3</sup>  
Gunasekaran Sethuraman<sup>4</sup> and Anbalagan Gopalakrishnan<sup>5\*</sup>

<sup>1</sup>Department of Physics, Dwaraka Doss Goverdhan Doss Vaishnav College,  
Arumbakkam, Chennai 600106, India

<sup>2</sup>Department of Physics, Veltech Dr. RR & Dr. SR Technical University,  
Avadi, Chennai 600062, India

<sup>3</sup>Institute of Low Temperature and Structure Research, Polish Academy of Sciences,  
50-950 Wrocław, 2, P.O. Box 937, Poland

<sup>4</sup>St. Peter's Institute of Higher Education and Research, St. Peter's University,  
Chennai 600054, India

<sup>5\*</sup> Department of Physics, Presidency College, Chennai 600005, India

\*Corresponding author: anbu24663@yahoo.co.in

**Abstract:** *Single crystals of melaminium phthalate (MPH) were grown from aqueous solution by slow solvent evaporation method at room temperature. X-ray powder diffraction analysis confirmed that the MPH crystal crystallises in orthorhombic system with space group Pbcn and the calculated lattice parameters were  $a = 33.559 \pm 0.066 \text{ \AA}$ ,  $b = 10.517 \pm 0.057 \text{ \AA}$ ,  $c = 7.117 \pm 0.025 \text{ \AA}$ ,  $\alpha = 90^\circ$ ,  $\beta = 90^\circ$ ,  $\gamma = 90^\circ$  and  $V = 2511.94 \text{ (\AA)}^3$ . The vibrational frequencies of various functional groups present in the MPH crystals have been derived from FIIR and FT-Raman analyses. The chemical structure of MPH was established by proton NMR and carbon NMR spectrum. The thermal decomposition behaviour of MPH has been studied by means of thermogravimetric analysis at three different heating rates 10, 15 and  $20^\circ\text{C min}^{-1}$ . The values of effective activation energy ( $E_a$ ) and pre exponential factor ( $\ln A$ ) of each stage were calculated by model free methods: Arrhenius, Flynn-Wall, Kissinger and Kim-Park method. A significant variation of effective activation energy ( $E_a$ ) with conversion ( $\alpha$ ) indicates that the process is kinetically complex. The linear relationship between the  $\ln A$  and  $E_a$  values was well established (compensation effect). No detectable signal was observed during second harmonic generation test.*

**Keywords:** Crystal growth, X-ray powder diffraction, FT-IR spectrum, FT-Raman spectrum, thermal analysis

### 1. INTRODUCTION

Melamine (2,4,6-triamino-1,3,5-triazine) has a wide range of applications in the industry. The use of melamine resin in automobile paints was examined by Zieba-Palus.<sup>1</sup> It is used as a fire retardant additive for polymeric materials and

readily forms insoluble adducts with many organic and inorganic acids.<sup>2</sup> Melamine is an industrial chemical mainly used in the production of melamine formaldehyde resins for surface coatings, laminates and adhesives and in the production of flame retardants resins to improve the flame resistance.<sup>3</sup> Melaminium phthalate crystal comprises mono-protonated melaminium ( $1^+$ ) residues and single dissociated hydrogen phthalate ( $1^-$ ) anions.

Generally, the solid-state complexation of melamine with different organic and inorganic (mineral) acids has an interesting aspect concerning the hydrogen bond system formed. Such a system comprises most frequently weak hydrogen bonds of N–H...O and O–H...O types.<sup>4</sup> Vibrational studies have been carried out by Marchewka.<sup>5</sup> Arenas and Marcos also published the infrared and Raman spectra of phthalic, isophthalic and tetraphthalic acids.<sup>6</sup> Additionally, several researchers have already examined the thermal behaviour of melamine.<sup>7-9</sup> Phase transformation of melamine at high pressure and temperature was studied by Yu et al.,<sup>10</sup> whereas Nagaishi et al.<sup>11</sup> analysed the thermal decomposition of the addition compound of melamine with hydrogen peroxide. Thermal and flame retardation properties of melamine phosphate-modified epoxy resins have been studied by Chen et al.<sup>12</sup> The presence of triazine ring in their structure gives improved hydrolytic and thermal stability.<sup>13</sup>

Kanagathara et al. reported the thermal decomposition behaviour of melaminium perchlorate monohydrate<sup>14</sup> and p-nitrophenol with melamine complex.<sup>15</sup> In the present work, we report the growth of melaminium phthalate (MPH) single crystal. The characterisations of the grown crystal were then made by XRD, Fourier transform infrared (FTIR) and FT-Raman studies. Thermal behaviour of kinetics has been carried out by thermogravimetric analysis at three different heating rates of 10, 15 and 20°C min<sup>-1</sup> and the results are discussed in later section.

## 2. EXPERIMENTAL

### 2.1 Materials and Methods

AR grade samples of melamine and phthalic acid were taken in 1:1 ratio. To the hot solution of melamine, the dissolved phthalic acid was added slowly and the solution was stirred well for about 6 h. Then the solution was filtered and allowed to evaporate at room temperature. The transparent single crystals were grown over a period of 30 days.

## 2.2 Characterisation

The grown crystals were characterised by X-ray powder diffraction technique using Rich Seifert X-ray powder diffractometer with  $\text{CuK}_\alpha$  radiation of  $\lambda = 1.5406 \text{ \AA}$ . The sample was scanned over the range of  $(2\theta) 10^\circ\text{--}80^\circ$  by employing the reflection mode. The detector used was a scintillation counter. Perkin Elmer Spectrum One FTIR spectrometer was employed to record the infrared spectrum to analyse the functional groups present in the crystals.

Raman spectral measurements were made with an FT-Raman Bruker RFS 27: S Raman module with a resolution of  $2 \text{ cm}^{-1}$ . An air cooled diode pumped Nd:YAG laser, operated at 1064 nm and a power output of 100 mW was used as source. The spectrum was recorded over the range of  $3500\text{--}50 \text{ cm}^{-1}$ . Proton NMR and carbon NMR spectra of title crystal were recorded using  $\text{D}_2\text{O}$  as solvent on a Bruker Avance III 500 MHz spectrometer at  $22^\circ\text{C}$  to confirm the molecular structure of the grown crystal.

The thermal behaviour of the crystal was determined by thermo gravimetric analysis and differential thermal analysis using SDT Q 6000 V 8.2 Built 100 thermal analyser at a heating rate of 10, 15 and  $20^\circ\text{C min}^{-1}$  under nitrogen atmosphere in the temperature range of  $30^\circ\text{C}\text{--}1000^\circ\text{C}$ . The grown crystal in its powder form was subjected to Kurtz second harmonic generation test by using Nd:YAG Q switched laser beam with input pulse of 0.68J for the non-linear optical property.

## 3. RESULTS AND DISCUSSION

### 3.1 X-ray Powder Diffraction Analysis

Figure 1 shows the indexed X-ray powder diffraction pattern of MPH crystal. X-ray powder diffraction analysis reveals that MPH crystallises in orthorhombic system with space group Pbcn. The calculated lattice parameters are  $a = 33.559 \pm 0.066 \text{ \AA}$ ,  $b = 10.517 \pm 0.057 \text{ \AA}$ ,  $c = 7.117 \pm 0.025 \text{ \AA}$ ,  $\alpha = 90^\circ$ ,  $\beta = 90^\circ$ ,  $\gamma = 90^\circ$  and  $V = 2511.94 (\text{ \AA})^3$ . The data reveal a close agreement with the reported values.<sup>4</sup>

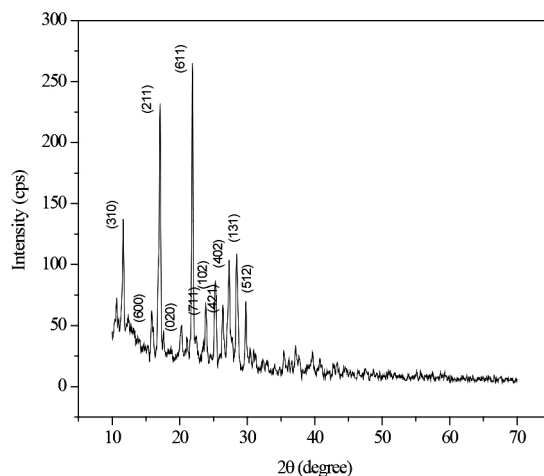


Figure 1: Powder X-ray diffraction pattern of MPH.

### 3.2 FTIR Studies

The FTIR spectrum of MPH is shown in Figure 2. The characteristic frequency of the functional groups present in the MPH crystal were assigned and tabulated in Table 1. The bands observed in the measured region arise from internal vibrations of melaminium cations and phthalate anions. Melaminium residues often form hydrogen bonds of N-H...N and N-H...O types. The NH<sub>2</sub> groups interact with the acid residue through weak N-H...O hydrogen bonds. The frequency of the band originating from this type of coupling rises from 3328 cm<sup>-1</sup> in the melamine crystal to 3393 cm<sup>-1</sup>.

In the present study, on addition of phthalic acid (ie) due to complex formation of MPH, an intense sharp peak at 3363 cm<sup>-1</sup> was observed. It might have occurred due to NH<sub>2</sub> asymmetric stretching vibration of three symmetric triazine NH<sub>2</sub> groups.<sup>16</sup> The peak at 2672 cm<sup>-1</sup> was due to side chain out of plane C-N bending vibration.<sup>16</sup> Bands appearing in the region of 1700–1540 cm<sup>-1</sup> was generally due to NH<sub>2</sub> group of melamine molecule as well as from C=O and COO<sup>-</sup> groups present in the compound. MPH consists of both non-dissociated (COOH) and ionised (COO<sup>-</sup>) carboxylic groups.<sup>4</sup>

Table 1: Vibrational band assignments for MPH crystal.

Wavenumber (cm <sup>-1</sup> )		Band assignments
Infrared	Raman	
3363		NH <sub>2</sub> asymmetric stretching
3115		N–H...O and N–H...N stretching
	3072	C–H stretch
	3063	C–H stretch
2672		Side chain out of plane C–N bend
1710	1695	C=O stretch
1670	1673	NH <sub>2</sub> bend or/and COO <sup>-</sup> stretch
1599	1599	Ring: Quadrant stretch and phthalate ring
1559	1575	COO <sup>-</sup> asymmetric stretch
1520		Side chain C–N asymmetric stretch
1361		O–H in plane bend
	1349	Ring: Semi-circle stretch
1309		Benzene CH deformation
1286		Carbonyl C–O stretch
1147	1148	Benzene C–H deformation
1080		Benzene C–C deformation
1051	1041	Ring breath and Benzene C=C stretch
989	983	Triazine ring N, in phase radial
810	807	C–C stretch
786		Ring-sextant out of plane bend
767		Ring-sextant out of plane bend
739		C=O in plane deformation
654	651	C=O out of plane bending
596, 576	572	Ring: Bend

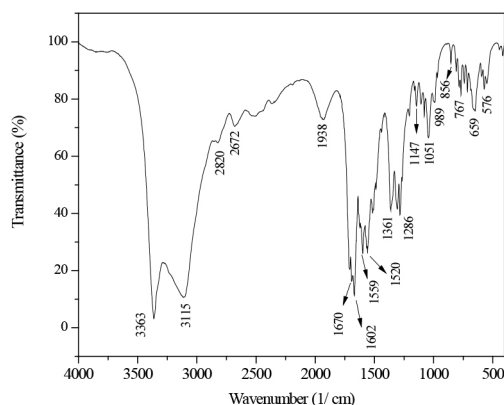


Figure 2: FTIR spectrum of MPH.

The band at  $1710\text{ cm}^{-1}$  was attributed to  $\text{COO}^-$  asymmetric stretching, whereas the bands at  $1670\text{ cm}^{-1}$  and  $1560\text{ cm}^{-1}$  were due to  $\text{NH}_2$  bend or  $\text{COO}^-$  stretch and  $\text{C=O}$  stretching, respectively.<sup>17,18</sup> The IR band at  $1361\text{ cm}^{-1}$  was assigned to O–H in plane bending type of vibration. Similar peak was observed at  $1365\text{ cm}^{-1}$  by Tarcan et al.<sup>19</sup> The strong peak at  $1599\text{ cm}^{-1}$  was due to ring quadrant stretch and phthalate ring.<sup>17</sup> The band at  $1051\text{ cm}^{-1}$  was assigned to triazine ring breathing mode of vibration,<sup>16</sup> while the band at  $989\text{ cm}^{-1}$  was attributed to triazine ring N, in-plane radial type of vibration.<sup>17</sup> This peak appeared for all melamine complexes. The IR peaks at  $739\text{ cm}^{-1}$  and  $654\text{ cm}^{-1}$  were attributed to  $\text{C=O}$  in plane deformation and  $\text{C=O}$  out of plane bending respectively.<sup>5</sup> Ring bending type of vibration occurs at  $586\text{ cm}^{-1}$  in the case of pure melamine. This peak was shifted to lower wave number  $574\text{ cm}^{-1}$  because of the addition of phthalic acid.

### 3.3 FT-Raman Studies

Figure 3 shows FT-Raman spectrum of MPH with the vibrational band assignments given in Table 1. The theoretical stretching frequencies of neutral melamine molecule were already reported by Fernandez et al.<sup>20</sup> and Meier et al.<sup>21,22</sup> C–H stretching vibrations were observed at  $3073\text{ cm}^{-1}$  and  $3063\text{ cm}^{-1}$ . The weak Raman band at  $983\text{ cm}^{-1}$  was due to triazine ring N in plane radial type of vibration.<sup>23</sup> This peak usually occurs between region of  $969\text{ cm}^{-1}$  and  $992\text{ cm}^{-1}$  for all melamine complexes.

In the case of melamine with trichloroacetic anion, this peak shifted to a lower wavenumber  $969\text{ cm}^{-1}$ , due to strong intermolecular interaction in between complex.<sup>24</sup> Similarly, the most intense band occurring at  $686\text{ cm}^{-1}$  was assigned to symmetric vibration of triazine ring. This band is the characteristic one for all melamine complexes.<sup>25</sup> Ring breathing and ring bending mode of vibrations were

observed at  $1041\text{ cm}^{-1}$  and  $572\text{ cm}^{-1}$  respectively.<sup>16</sup> Also, C–H deformation of benzene ring occurs at  $1148\text{ cm}^{-1}$ . The peak at  $1673\text{ cm}^{-1}$  was due to either  $\text{NH}_2$  bending vibration of melamine or  $\text{COO}^-$  structures. The band at  $651\text{ cm}^{-1}$  was due to C=O out of plane bending vibration.<sup>5,24</sup>

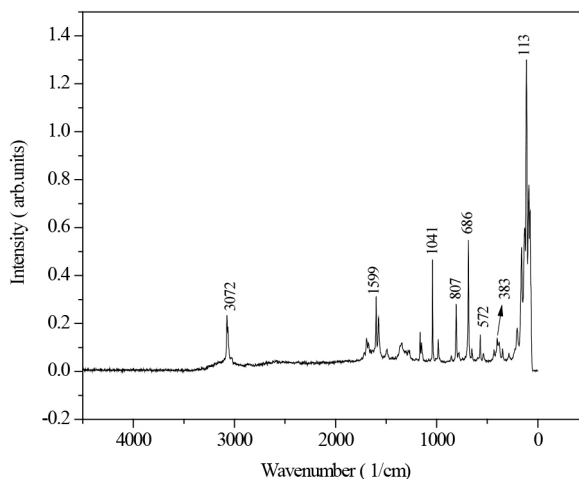


Figure 3: FT-Raman spectrum of MPH.

### 3.4 FT-NMR Studies

The  $^1\text{H}$  NMR and  $^{13}\text{C}$  NMR spectral analysis are the important analytical techniques used to study the structure of organic compounds. The  $^1\text{H}$  NMR and  $^{13}\text{C}$  NMR spectra of MPH crystal are presented in Figure 4 and Figure 5 respectively. The signals due to N–H and COOH protons did not show up because of fast deuterium exchange taking place in these two groups with  $\text{D}_2\text{O}$  being used as the solvent.<sup>26</sup> Due to hygroscopic nature of the title crystal, strong intense water signal appeared at 4.680 ppm. The two different proton environments showed peaks at 7.456 and 7.600 ppm. From the  $^{13}\text{C}$  NMR spectrum, the signal at 128.57 ppm is due to 3 carbon atoms present in the triazine ring. The presence of phthalic acid is confirmed by the presence of peak at 130.61 ppm.

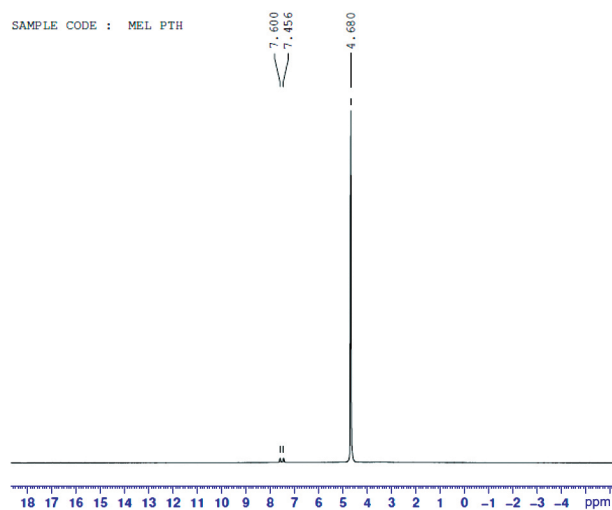


Figure 4: Proton NMR spectrum of MPH.

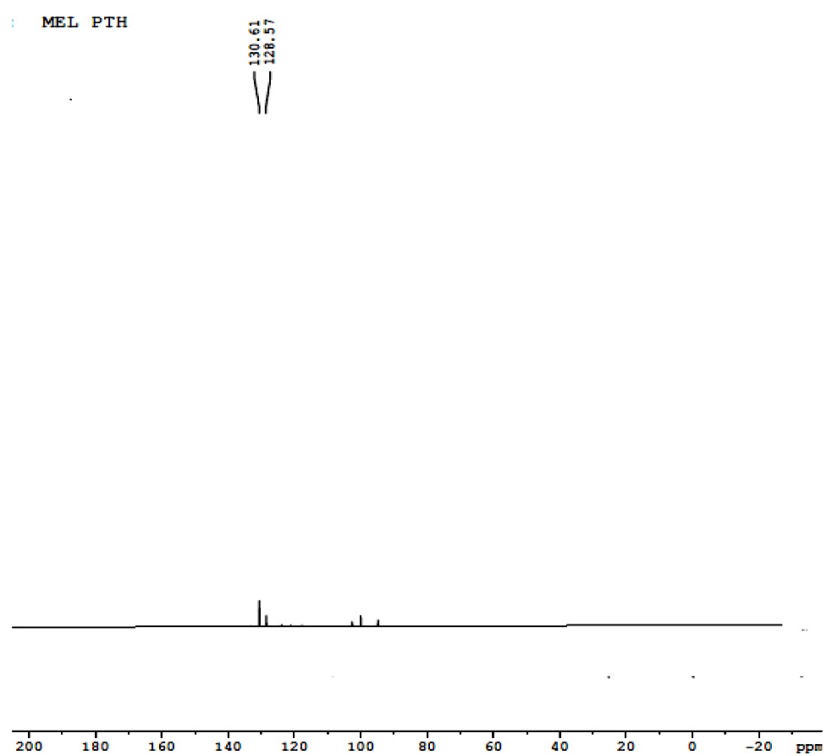


Figure 5: Carbon NMR spectrum of MPH.



### 3.5 SHG Studies

Second harmonic generation test was performed to find the NLO property of the grown crystal by using Kurtz-Perry technique.<sup>27</sup> Kurtz technique is used as a screening technique to identify materials with the capability for phase matching in addition to identifying materials with non centrosymmetric crystal structure. Crystals were grounded into powder and densely packed in between two glass slides. Nd:YAG laser using the first harmonics output of 1064 nm with pulse width of 8 ns and repetition rate 10 Hz was passed through the sample. KDP was taken as a reference material. When a laser input of 0.68J was passed through the sample, there was no emission of green signal. Usually centrosymmetric crystals do not show second harmonic generation effect.<sup>28</sup>

### 3.6 Thermal Analysis

Thermogravimetric analysis (TG) is an effective tool to characterise thermal stability of a variety of products.<sup>29,30</sup> TG-DTG curves of MPH at three different heating rates of  $10^{\circ}\text{C min}^{-1}$ ,  $15^{\circ}\text{C min}^{-1}$  and  $20^{\circ}\text{C min}^{-1}$  in the temperature range of  $30^{\circ}\text{C}$ – $1000^{\circ}\text{C}$  are shown in Figure 6. It is seen from the figure that the decomposition of MPH occurred in two stages. There was no mass loss observed around  $100^{\circ}\text{C}$  which indicated the absence of water molecule in MPH. For heating rate  $20^{\circ}\text{C min}^{-1}$ , the initial mass taken was 1.6300 mg.

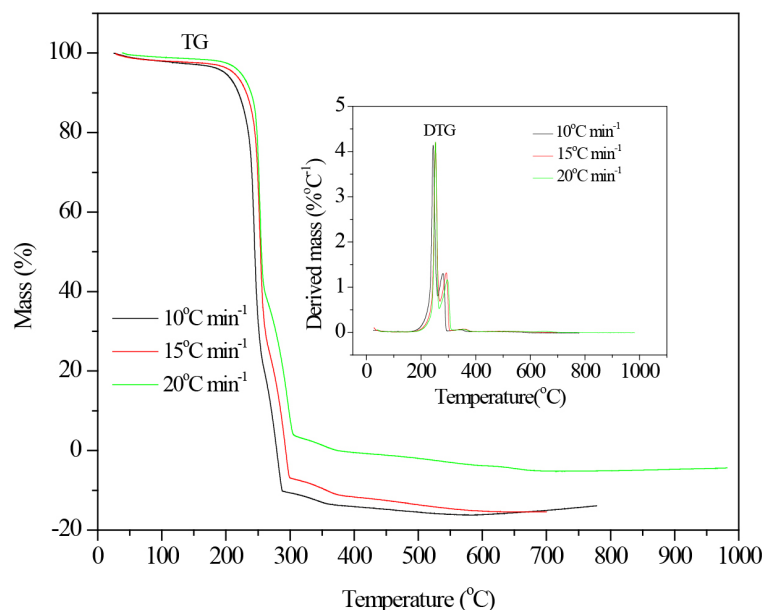


Figure 6: TG-DTG curves of MPH in nitrogen atmosphere, at different heating rates of  $10^{\circ}\text{C min}^{-1}$ ,  $15^{\circ}\text{C min}^{-1}$  and  $20^{\circ}\text{C min}^{-1}$ .

The first stage of decomposition was accompanied by a rapid weight loss that took place in the temperature range of between 245.98°C and 255.73°C, with a weight loss of 63.40%. This weight loss was due to the decomposition of phthalate molecule from the compound structure. It exactly matches an exothermic peak at 253.6°C in DTG curve which is assigned as the melting point of MPH. The remaining 33.60% of weight loss occurring in the 285.56°C–303.22°C range was due to the decomposition of melamine with a final residue of 0.002921 mg. This was accompanied by an exothermic peak at 296.5°C.

Generally, thermal decomposition of melamine happens in stages and is accompanied by the detachment of ammonia. Melamine first decomposes into melam and then melon. The NH<sub>2</sub> groups in melam can be replaced by other atoms and groups.<sup>31</sup> In the experiment, the melting point was found to be high indicating that MPH has better thermal stability which makes it suitable for thermal applications. Figure 6 above shows the TG-DTG curves of MPH in nitrogen atmosphere at three different heating rates. Heating rate is one of the most important parameters affecting the chemical reactions. Reaction kinetics can be substantially altered by changing the heating rate over a wide range.

It is seen from Figure 6 that TG curves shifted to higher temperatures as the heating rate was increased. This shows that definite heating rate influences the thermal decomposition.<sup>32</sup> Polymer molecules did not have enough time to absorb the heat and reach thermal equilibrium. As the heating rate was increased, the degradation rate slowed down. Since the experiment was carried out under nitrogen atmosphere, DTG curve showed a single peak implying that the thermal decomposition process occurred in a single step. When the heating rate was increased from 10°C min<sup>-1</sup> to 20°C min<sup>-1</sup>, the phthalate thermal decomposition temperatures shifted to higher temperature from 245°C to 252°C respectively. Similarly, melaminium thermal decomposition temperature shifted from 280°C to 296°C respectively. Thus, as the heating rate was increased, the temperature at initial thermal decomposition and the maximum decomposition rate shifted towards a higher temperature.

### 3.7 TG Kinetics Method of Thermal Degradation

A large number of mathematical models have been proposed and used for studying kinetics and mechanism of such reactions using the TG data. Multiple heating rate data have been recommended for non-isothermal studies.<sup>33</sup> Here, we studied the kinetics of the thermal decomposition of MPH at three different heating rates by three different multiple heating methods, i.e., Flynn-Wall, Kissinger and Kim-Park.<sup>34–36</sup>

The rate of degradation  $\frac{d\alpha}{dt}$  can be expressed as the product of the function of temperature and the function of conversion. Typical graphs depicting fraction reacted,  $\alpha$  versus temperature for two stages are shown in Figure 7. Flynn-Wall plots for three different heating rates against the temperature for stages I and II are shown in Figure 8. The straight lines obtained were nearly parallel to each other. At each heating rate, the temperatures were determined corresponding to extents of overall conversion of 0.05–0.65 in intervals of 0.05.

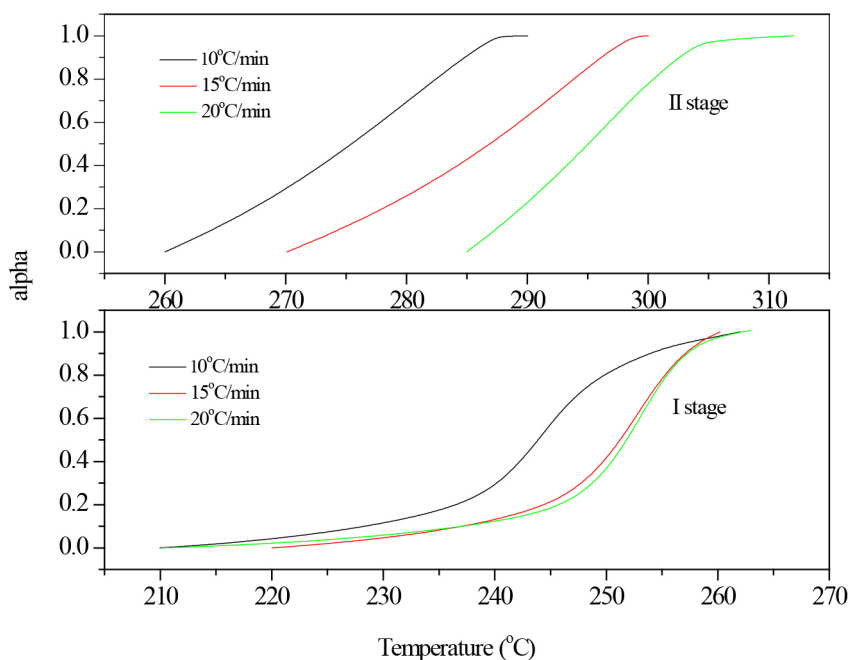


Figure 7: Fraction reacted,  $\alpha$  versus temperature for stages I and II at three different heating rates.

Activation energy ( $E_a$ ) was calculated from the slope of the plot  $\ln \beta$  against  $1/T$  for a fixed mass loss and the values are tabulated in Table 2. The linear Arrhenius plots of  $\ln k$  versus  $1/T$  for the thermal decomposition of MPH at three different heating are shown in Figure 9. From the slope of the Arrhenius plots, the  $E_a$  for both stages have been calculated and are listed in Table 3. Also, activation energies have been calculated using Kissinger and Kim-Park methods and the results are compared in the Table 3.

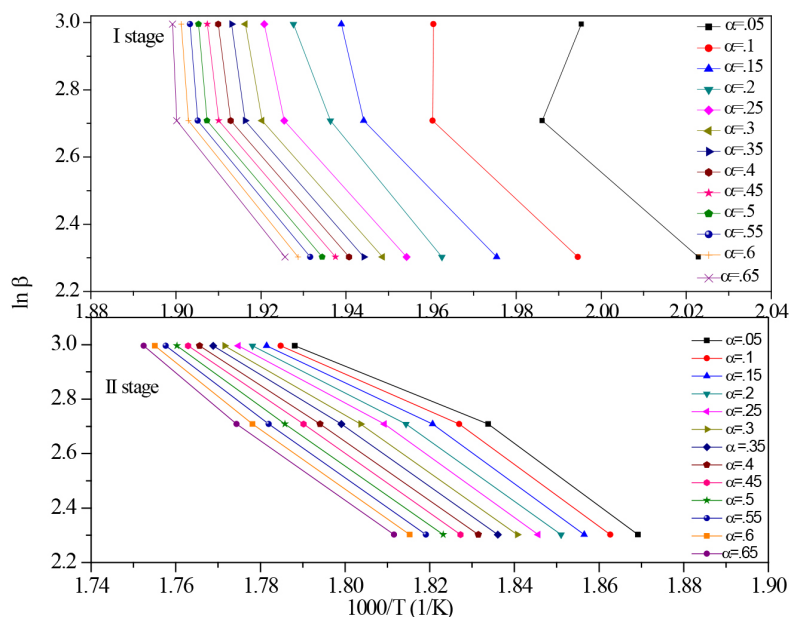


Figure 8: Flynn-Wall plot for stage I and II in nitrogen atmosphere for non-isothermal decomposition of MPH using TG data.

Table 2: Kinetic parameters of non-isothermal decomposition of MPH by Flynn-Wall method.

$\alpha$	Flynn-Wall method			
	Stage I		Stage II	
	$E_a$ (kJ mol <sup>-1</sup> )	ln A (s <sup>-1</sup> )	$E_a$ (kJ mol <sup>-1</sup> )	ln A (s <sup>-1</sup> )
0.05	118.83	28.61	70.22	15.99
0.1	133.89	31.64	73.51	16.62
0.15	140.41	32.82	76.56	17.2
0.2	156.69	36.33	79.08	17.67
0.25	152.79	35.29	81.45	18.12
0.3	156.55	36.04	83.57	18.51
0.35	159.86	36.71	85.93	18.95
0.4	160.77	36.86	87.63	19.25
0.45	163.24	35.05	89.62	19.62
0.5	166.57	38.05	91.56	19.98
0.55	170.69	38.93	93.58	20.35
0.6	175.19	39.89	95.2	20.64
0.65	178.65	40.6	96.72	20.91

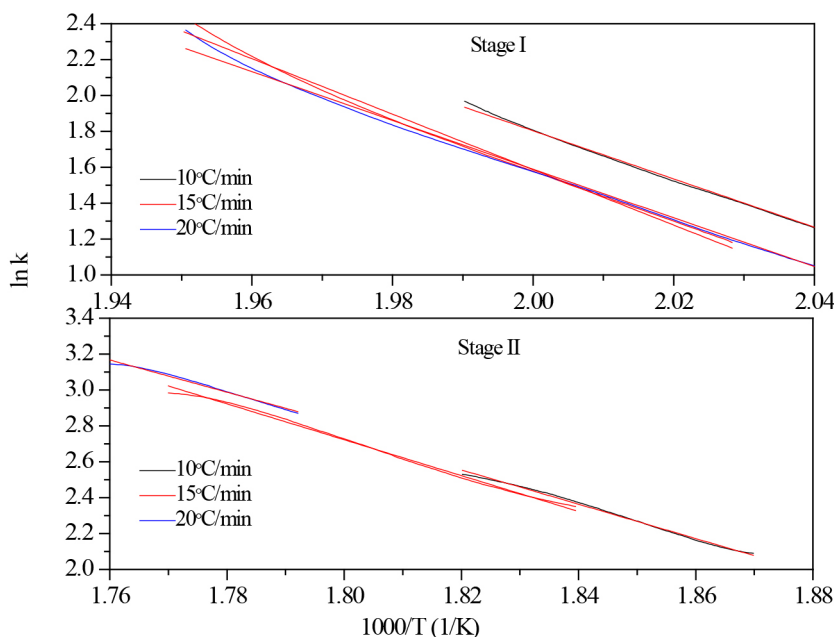


Figure 9: Arrhenius plot for stage I and II for non-isothermal decomposition of MPH.

Table 3: Activation energies for the thermal degradation of MPH by Arrhenius, Kissinger and Kim-Park methods.

Method	Heating rate (°C min <sup>-1</sup> )	Stage I		Stage II	
		E <sub>a</sub> (kJ mol <sup>-1</sup> )	ln A (s <sup>-1</sup> )	E <sub>a</sub> (kJ mol <sup>-1</sup> )	ln A (s <sup>-1</sup> )
Arrhenius	10	111.63	28.65	79.52	19.96
	15	128.49	32.49	83.10	20.71
	20	112.89	28.74	74.54	18.94
Kissinger		130.59	20.15	104.37	12.29
Kim-Park		139.29	34.67	113.72	26.96

All the three methods yielded similar calculation results. The values of E<sub>a</sub> are within the range < 60 kJ mol<sup>-1</sup> as expected for removal of weakly bound water of crystallisation from such compounds.<sup>37,38</sup> Therefore, it can be assumed that the water of crystallisation was not present in MPH. E<sub>a</sub> of MPH was found to be higher than that of melamine with other complexes.<sup>14,15</sup> The effective E<sub>a</sub> can vary strongly with the temperature and the extent of conversion.<sup>37</sup> If the effective E<sub>a</sub> is roughly constant over the entire conversion range, then it is said to be dominated by a single step mechanism.

In the present case, it can be seen from Figure 10(a) that during both stages of decomposition, a significant variation in effective  $E_a$  with conversion ( $\alpha$ ) indicates that the process is kinetically complex, i.e., multi-step reaction mechanism.<sup>38</sup> Polymers and other complex organic materials tend to have increase in  $\ln A$  and  $E_a$  as conversion increases. This is consistent with the residual material becoming increasingly refractory.<sup>33</sup>

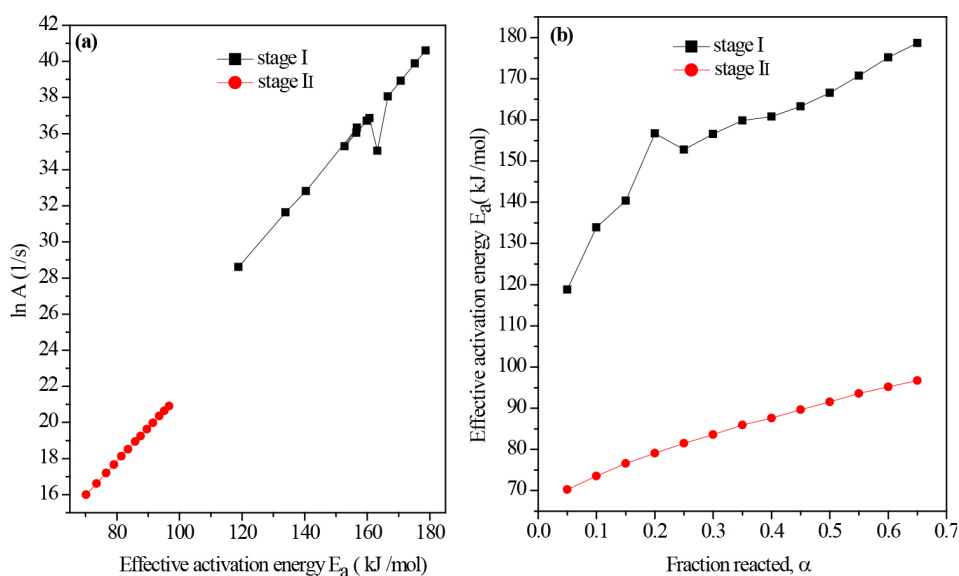


Figure 10: Illustration of (a) plot of pre-exponential factor ( $\ln A$ ) versus effective  $E_a$ ; and (b) variation of effective  $E_a$  versus fraction reacted ( $\alpha$ ) by Flynn-Wall method for stages I and II.

In the present study, there was a steady increase in  $\ln A$  and  $E_a$  as the conversion increased. This suggests that MPH can be a good polymeric material. Dependence of effective  $E_a$  on  $\alpha$  was used to identify its kinetic scheme, i.e., these values were used for input to multi-step for model fitting purposes.<sup>38</sup> Kinetic compensation effect was observed in many isothermal processes. The value of  $E_a$  bears a linear relationship with  $\ln A$ :

$$\ln A = aE_a + b \quad (1)$$

where  $a$  and  $b$  are compensation parameters. For stage I, the calculated compensation parameters are  $a = 5.3858$ ,  $b = 0.1951$  and for stage II,  $a = 3.0611$  and  $b = 0.1847$ . The compensation effect is well established for the thermal decomposition of MPH and it is shown in Figure 10(b). Kinetic analysis of TG data based on the rate equation:

$$\beta d\alpha/dt = A \exp(-E/RT) f(\alpha) \quad (2)$$

which states that the rate of the reaction is proportional to the rate coefficient with Arrhenius temperature dependence and a function of the degree of conversion. The integral form of equation is given by the expression

$$\ln [g(\alpha)/T^2] = \ln [(AR/\beta E_a)(1-2RT/E_a)] - E_a/RT \quad (3)$$

where  $A$  is the pre-exponential factor,  $E_a$  is the effective activation energy and  $R$  is the gas constant. Several researchers<sup>14,15,39,40</sup> reported the kinetic analysis by model fitting methods and dissociation mechanisms. In the present study, all kinetic models (P4, P3, P2, P2/3, D1, F1, A4, A3, A2, D3, R3, R2 and D2) have been tested for all the two stages. A plot of  $\ln [g(\alpha)/T^2]$  versus  $1000/T$  gives a straight line when the correct  $g(\alpha)$  function is used in the equation is shown in Figure 11. This  $g(\alpha)$  function gives the mechanism of the reaction. Straight line with high correlation coefficient and low standard deviation values are selected to represent the possible controlling mechanism.

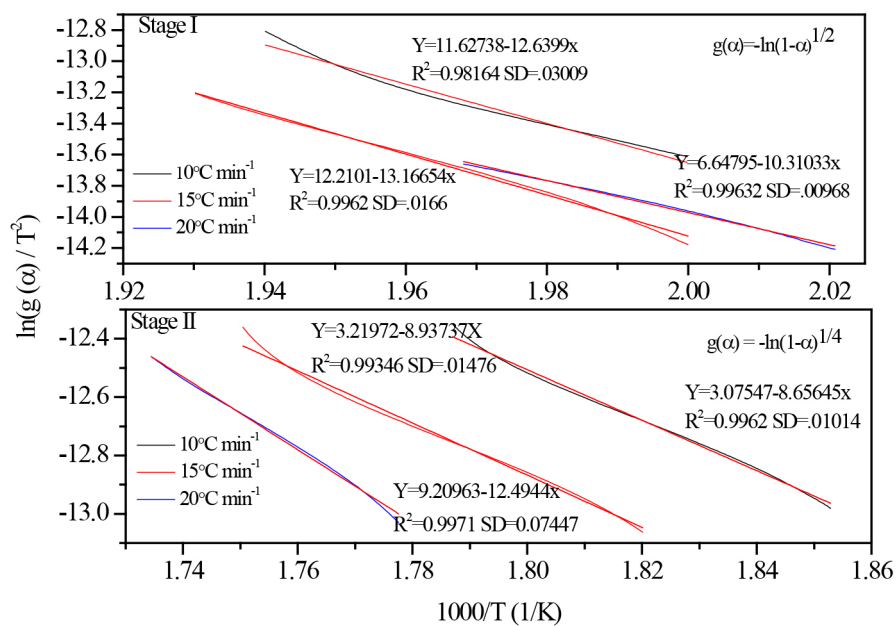


Figure 11: Plot of  $\ln[g(\alpha)/T^2]$  versus  $1000/T$  for stages I and II using TG data.

The non isothermal kinetic data of MPH crystal between the limit of  $\alpha$  from 0 to 0.65 have been fitted to all reaction models. More than one model (A2, A4) gave a very good coefficient of linear equation lines with high correlation coefficient and low standard deviation value. However, by comparing the  $E_a$

values with the model-free method, it is found that stage I is accepted by Avrami-Erofeev's model (A2) and the stage II was accepted by Avrami-Erofeev's (A4) model. The values of  $E_a$ , pre-exponential factor ( $\ln A$ ), coefficient of correlation  $R$  and standard deviation at three different heating rates for two stages are presented in Table 4.

Table 4: Kinetic parameters and possible rate controlling processes of decomposition of MPH.

Kinetic model	Heating rate ( $^{\circ}\text{C min}^{-1}$ )	$E_a$ ( $\text{kJ mol}^{-1}$ )	$\ln A$ ( $\text{s}^{-1}$ )	Correlation Coefficient, $R$	Std. Deviation
A2	10	105.09	11.63	0.99077	0.03009
	15	109.47	12.21	0.99809	0.0166
	20	85.73	6.65	0.99815	0.00968
A4	10	71.97	3.07	0.99810	0.01014
	15	74.30	3.22	0.99672	0.01476
	20	103.88	9.21	0.99854	0.07447

The Arrhenius parameters ( $E_a$ ,  $\ln A$ ) of decomposition are highly variable, exhibiting a strong dependence on the reaction model chosen. Similarly, pre-exponential values also change with the heating rate. The real activation energy for each stage of decomposition can be obtained only at lowest heating rate.

#### 4. CONCLUSION

Single crystals of melaminium phthalate were grown by slow solvent evaporation technique. The grown crystals were characterised by X-ray diffraction and it was found that it crystallised in the space group  $Pbcn$  with orthorhombic geometry. The calculated lattice parameter values were comparable with the reported value. The various infrared and Raman bands derived from internal vibrations of melaminium cations and phthalate anions were assigned for the grown crystal. Several stretching and deformation modes confirm the presence of extensive intermolecular hydrogen bonding in the crystal. FT-NMR spectroscopic analysis confirms the molecular structure of the grown compound.

No detectable signal was observed during second harmonic generation test. Thermo gravimetric measurements were carried out at three different heating rates  $10^{\circ}\text{C min}^{-1}$ ,  $15^{\circ}\text{C min}^{-1}$  and  $20^{\circ}\text{C min}^{-1}$ . Multiple heating rate methods, i.e., Flynn-Wall, Kissinger and Kim-Park were used for kinetic calculations. The effective activation energies obtained by these methods were comparable. The activation energy obtained from Kim-Park method was higher than those from



other methods. A significant variation between  $E_a$  versus  $\ln A$  indicates that the system follows multistep mechanism. Compensation effect was well established. From the results, it is concluded that Avrami Erofeev's model (A2) is the most probable kinetic model for thermal decomposition of MPH for the stage I and Avrami Erofeev's model (A4) for stage II.

## 5. REFERENCES

1. Zieba-Palus, J. (1999). Application of micro-Fourier transform infrared spectroscopy to the examination of paint samples. *J. Mol. Struct.*, 511, 327–335.
2. Crews, G. M. et al. (2001) Melamine and guanamines. In Diem, H. & Matthias, G. (Eds.). *Ullmann's encyclopedia of industrial chemistry*, 6th ed. Weinheim: Wiley-VCH Verlag.
3. Dirk, J. A. et al. (2004). Crystal structure of melaminium orthophosphate from high-resolution synchrotron powder-diffraction data. *Helv. Chim. Acta*, 87, 1894–1904.
4. Janczak, J. & Perpetuo, G. J. (2001). Melaminium phthalate. *Acta Cryst. C*, 57, 123–125.
5. Marchewka, M. K. (2004). Infrared and Raman spectra of the new melaminium salt: 2,4,6-triamino-1,3,5-triazin-1-ium hydrogenphthalate. *Mater. Lett.*, 58, 843–848.
6. Arenas, J. F. & Marcos, J. I. (1980). Infrared and Raman spectra of phthalic isophthalic and terephthalic acids. *Spectrochim. Acta A*, 36, 1075–1081.
7. May, H. (1959). Pyrolysis of melamine. *J. Appl. Chem.*, 9, 340–344.
8. Vander Pleats, G., Soons, H. & Snellings, R., (1981). Second European symposium on thermal analysis, London, 1–4 September, 215–218.
9. Costa, L. & Camino, G. (1988). Thermal behavior of melamine. *J. Therm. Anal.*, 34, 423–429.
10. Yu, D. L. et al. (2008). Phase transformation of melamine at high pressure and temperature. *J. Mater. Sci.*, 43, 689–695.
11. Nagaishi, T. et al. (1990). Thermal decomposition of addition compound of melamine with hydrogen peroxide. *J. Therm. Anal.*, 36, 55–60.
12. Chen, W-Y., Wang, Y-Z. & Chang, F-E. (2004). Thermal and flame retardation properties of melamine phosphate-modified epoxy resins. *J. Polym. Res.*, 11, 109–117.
13. Siimer, K. et al. (2008). TG-DTA study of melamine-urea-formaldehyde resins. *J. Therm. Anal. Calorim.*, 92, 19–27.
14. Kanagathara, N. et al. (2012). A study of thermal and dielectric behavior melaminium perchlorate monohydrate single crystals. *J. Therm. Anal. Calorim.*, DOI: 10.1007/s10973-012-2713-8.

15. Kanagathara, N. (N. D.). Thermal decomposition of bis(4-nitrophenol)-2,4,6 triamino 1,3,5 triazine monohydrate. Unpublished data.
16. Jones, W. J. & Orville-Thomas, W. J. (1959). The infra-red spectrum and structure of dicyandiamide. *Trans. Faraday Soc.*, 55, 193–202.
17. Larkin, P. J. et al. (1998). Vibrational analysis of some important group frequencies of melamine derivatives containing methoxymethyl and carbamate substituents: Mechanical coupling of substituent vibrations with triazine ring modes. *Vib. Spectrosc.*, 17, 53–72.
18. Loring, J. S. et al. (2001). Infrared spectra of phthalic acid, the hydrogen phthalate ion and the phthalate ion in aqueous solution. *Spectrochim. Acta A*, 57, 1635–1642.
19. Tarcan, E. et al. (2008). Molecular structure and vibrational assignment of melaminium phthalate by density functional theory (DFT) and ab initio Hartree-Fock (HF) calculations. *Spectrochim. Acta A*, 1, 169–174.
20. Fernandez-Liencres, M. P. et al. (2001). Measurement and ab initio modelling of the inelastic neutron scattering of solid melamine: Evidence of the anisotropy in the external modes spectrum. *Chem. Phys.*, 266, 1–17.
21. Meier, R. J., Tiller, A. & Vanhommerig, S. A. M. (1995). Molecular modelling of melamine-formaldehyde resins. 2. Vibrational spectra of methylolmelamines and bridged methylolmelamines. *J. Phys. Chem.*, 99, 5457–5464.
22. Meier, R. J. et al. (1995). Molecular modelling urea and melamine formaldehyde resins. 1. A force field for urea and melamine. *J. Phys. Chem.*, 99, 5445–5446.
23. Larkin, P. J., Makowski, M. P. & Colthoupe, N. B. (1999). The form of the normal modes of s-triazine: Infrared and Raman spectral analysis and ab initio force field calculations. *Spectrochim. Acta A*, 55, 1011–1020.
24. Kanagathara, N. et al. (2013). Growth and characterization of Melaminium bis(trichloroacetate) dehydrate. *Spectrochim. Acta A*, 101, 112–118.
25. Marchewka, M. K. (2003). Infrared and Raman spectra of Melaminium bis(4-hydroxybenzenesulfonate) dehydrate. *Acta Chim. Solv.*, 50, 239–250.
26. Dirk, W. et al. (2009). NMR-spectroscopy for nontargeted screening and simultaneous quantification of health-relevant compounds in foods: The example of melamine. *J. Agri. Food Chem.*, 57, 7194–7199.
27. Kurtz, S. K. & Perry, T. T. (1968). Powder technique for the evaluation for the nonlinear optical materials. *J. Appl. Phys.*, 39, 3798–3813.
28. Dmitriev, V. G., Gurzadyan, G. G. & Nikogosyan, D. N. (1997). *Handbook of nonlinear optical crystals*, 2nd ed. Berlin: Springer.
29. Paul, G. (2008). *Principles and applications of thermal analysis*. Oxford: Blackwell.

30. Brown, M. E. (2003) *Handbook of thermal analysis and calorimetry*, vol.1. Amsterdam: Elsevier.
31. Franklin, E. C. (1922). The ammono carbonic acids. *J. Am. Chem. Soc.*, 44, 486–509.
32. Sang, M. S. & Seong, H. K. (2009). Thermal decomposition behavior and durability evaluation of thermotropic liquid crystalline polymers. *Macromol. Res.*, 17, 149–155.
33. Vyazovkin, S. et al. (2011). ICTAC kinetics committee recommendations for performing kinetic computations on thermal analysis data. *Thermochim. Acta*, 520, 1–19.
34. Flynn, J. H. & Wall, L. A. (1966). A quick, direct method for the determination of activation energy from thermogravimetric data. *J. Polym. Sci. B*, 4, 323–328.
35. Kissinger, H. E. (1957). Reaction kinetics in differential thermal analysis. *Anal. Chem.*, 27, 1702–1706.
36. Kim, S. & Park, J. K. (1995). Characterization of thermal reaction by peak temperature and height of DTG curves. *Thermochim. Acta*, 264, 137–156.
37. Balboul, B. A. A. et al. (2002). Non-isothermal studies of the decomposition course of lanthanum oxalate decahydrate. *Thermochim. Acta*, 387, 109–114.
38. Brown, M. E., Dollimore, D. & Galwey, A. K. (1980). *Reactions in solid state*. Amsterdam: Elsevier.
39. Rajendran, J. et al. (2011). Kinetics and dissociation mechanism of heptaaqua-p-nitrophenolato strontium (II) nitrophenol. *J. Therm. Anal. Calorim.*, 103, 845–851.
40. Jankovic, B., Mentus, S. & Jankovic, M. (2008). A kinetic study of the thermal decomposition process of potassium metabisulfite: Estimation of distributed reactivity model. *J. Phys. Chem. Solids*, 69, 1923–1933.